ALPHA PARTICLE DESTABILIZATION OF THE TOROIDICITY-INDUCED ALFVEN EIGENMODES

C. Z. Cheng

PPPL--2717

DE91 000486

Princeton Plasma Physics Laboratory
Princeton University, Princeton, NJ 08543 USA

Abstract

The high frequency, low mode number toroidicity-induced Alfven eigenmodes (TAE) are shown to be driven unstable by the circulating and/or trapped α-particles through the wave-particle resonances. Satisfying the resonance condition requires that the α-particle birth speed $v_\alpha \geq v_A/2|m-nq|$, where v_A is the Alfven speed, m is the poloidal mode number, and n is the toroidal mode number. To destabilize the TAE modes, the inverse Landau damping associated with the α-particle pressure gradient free energy must overcome the velocity space Landau damping due to both the α-particles and the core electrons and ions. The growth rate was studied analytically with a perturbative formula derived from the quadratic dispersion relation, and numerically with the aid of the NOVA-K code. Stability criteria in terms of the α-particle beta β_α, α-particle pressure gradient parameter (ω_*/ω_A) (ω_* is the α-particle diamagnetic drift frequency), and (v_α/v_A) parameters will be presented for TFTR, CIT, and ITER tokamaks. The volume averaged α-particle beta threshold for TAE instability also depends sensitively on the core electron and ion temperature. Typically the volume averaged α-particle beta threshold is in the order of 10^{-4}. Typical growth rates of the n=1 TAE mode can be in the order of $10^{-2}\omega_A$, where $\omega_A = v_A/qR$. Other types of global Alfven waves are stable in D-T tokamaks due to toroidal coupling effects.

I. Introduction

Among the major issues in the α-particle physics of tokamaks operating with deteurium-tritium (D-T) are the α-particle driven global MHD instabilities and the resultant α-particle transport. If large amplitude global MHD modes are excited, they can cause anomalous α-particle losses, severely affecting the tokamak reactor operations. The low-n toroidicity-induced Alfven eigenmode (TAE)[1] is considered to be one of the most serious instabilities driven by the α-particles in D-T tokamaks such as the Tokamak Fusion Test Reactor (TFTR), the Compact Ignition Tokamak (CIT), and the International Thermonuclear Experimental Reactor (ITER). The destabilization effects of α-particles on the TAE modes had previously been studied[2-6] by analytical theories as well as numerical computations using the NOVA-K code.[7] For the TAE modes with frequency $\omega \sim v_A/2qR \sim \omega_t, \omega_b$ (v_A is the Alfven speed, q is the safety factor, R is the tokamak major radius, ω_t is the circulating α-particle transit frequency, and ω_b is the trapped α-particle bounce frequency), the ideal MHD stable global Alfven modes can be driven unstable by the α-particles through bounce or transit resonances with the background waves. Alpha particles may destabilize the TAE modes through wave-particle resonances by tapping the free energy associated with the α-particle pressure nouniformity. Satisfying the resonance condition requires that the α-particle birth speed $v_\alpha \geq v_A / 2 |m - nq|$, where m is the poloidal harmonic and n is the toroidal mode number. To destabilize the TAE modes, the inverse Landau damping associated with the α-particle pressure gradient free energy must overcome the velocity space Landau damping. Typical growth rates of the n=1 TAE mode[2-6] can be on the order of $10^{-2}\omega_A$, where $\omega_A = v_A/qR$. Other types of global Alfven waves had been shown to be stable in D-T tokamaks due to toroidal coupling effects.[3,8]

The anomalous α-particle losses due to the TAE modes had been investigated by using a Hamiltonian guiding center orbit Monte Carlo code.[9] Significant α-particle losses were found when the fluctuation level of the global MHD modes is large with $(\delta B_r/B) \geq 10^{-4}$. Whereas the low frequency internal kink (fishbone) modes are responsible for the anomalous losses of the trapped α-particles, the high frequency TAE modes affect the transport of the untrapped α-particles. Circulating α-particles that resonate with the TAE modes will lose energy and increase their radial outward excursions. Near the edge, they can become trapped and enter prompt-loss banana orbits. The α-particle loss rate, computed from the Hamiltonian guiding center orbit code, scales roughly linearly with $(\delta B_r/B)$. For $(\delta B_r/B) = 5 \times 10^{-4}$ the α-particle loss time is appreciably shorter than the α-particle slowing-down time. If the α-particles excite both the n=1 and n=2 TAE modes, their losses will be enhanced due to stochastic particle orbit losses.

In this paper the stability property of the TAE mode is studied extensively with a perturbative analysis based on a quadratic dispersion relation and numerically with the aid of the NOVA-K code. The stabilizing resonance effects due to core electrons and ions are also included. For D-T tokamaks the volume averaged α-particle beta threshold for TAE instability is small and is on the order of 10^{-4}. In the following, we briefly describe in Sec. II the formulation of the kinetic-MHD eigenmode equations which included the kinetic effects due to all plasma species. A quadratic form is derived for the kinetic-MHD eigenmode equations in Sec. III. In Sec. IV, we present a perturbative analysis of the α-particle destabilization of TAE modes via wave-particle resonances. We describe the Alfvén waves in tokamaks and the existence of the TAE modes in Sec. IV.A. An analytical local stability criterion for the driven TAE modes that takes into account the stabilizing core electron and ion Landau dampings is given in Sec. IV.B. Stability diagrams computed from the global stability analysis are presented in Sec. IV.C in terms of the β_α and (v_α/v_A) parameters for the TFTR, CIT, and ITER tokamaks. The principal conclusions of this work are presented and future improvements over the TAE stability calculations are discussed in Sec. V.

II. Formulation of Kinetic-MHD Stability Equations

In terms of the flux coordinate system (ψ,θ,ζ), the equilibrium magnetic field with nested flux surfaces can be written as

$$\vec{B} = \nabla\zeta \times \nabla\psi + q(\psi)\, \nabla\psi \times \nabla\theta, \tag{1}$$

where $2\pi\psi$ is the poloidal flux within a magnetic surface, $q(\psi)$ is the safety factor, θ is the generalized poloidal angle varying between 0 and 2π, and ζ is the generalized toroidal angle varying between 0 and 2π. Since

$$\vec{B} \bullet \nabla = J^{-1} \left(\frac{\partial}{\partial\theta} + q \frac{\partial}{\partial\zeta} \right), \tag{2}$$

where $J = (\nabla\psi \times \nabla\theta \bullet \nabla\phi)^{-1}$ is the Jacobian, the magnetic field lines are straight in this coordinate system. For axisymmetric equilibria, $\vec{B}$ can also be expressed as

$$\vec{B} = \nabla\phi \times \nabla\psi + g\, \nabla\phi, \tag{3}$$

where $g = X B_\phi$, B_ϕ is the toroidal magnetic field, ϕ is the toroidal angle in cylindrical (X,ϕ,Z) coordinates. Then, ζ is related to ϕ by

$$\zeta = \phi - q\,\delta(\theta,\psi)\,, \tag{4}$$

where $\delta(\theta,\psi)$ is periodic in θ and is determined by

$$q\,(1 + \partial\delta/\partial\theta) = g\,J / X^2\,. \tag{5}$$

We consider stationary isotropic ideal MHD equilibria satisfying

$$\vec{J} \times \vec{B} = \nabla P\,, \tag{6}$$

$$\nabla \times \vec{B} = \vec{J}\,, \tag{7}$$

$$\nabla \bullet \vec{B} = 0\,, \tag{8}$$

where $\vec{J}$, $\vec{B}$, and P are the equilibrium current, magnetic field, and pressure, respectively.

We will consider an axisymmetric toroidal plasma consisting of the core and alpha components with $n_\alpha << n_c$ and $T_\alpha >> T_c$ so that $\beta_\alpha < \beta_c$. Summing the collisionless equations of motion for each species, we obtain the linear momentum equation

$$\omega^2 \rho\,\vec{\xi} = \nabla \bullet \delta\vec{\vec{P}} + \vec{b} \times (\nabla \times \vec{B}) + \vec{B} \times (\nabla \times \vec{b})\,, \tag{9}$$

where $\vec{\xi}$ is the usual fluid displacement vector, $\vec{b}$ is the perturbed magnetic field, $\delta\vec{\vec{P}}$ is the total perturbed particle pressure tensor due to all species, and ρ is the total plasma mass density. The following ideal MHD relations hold

$$\vec{b} = \nabla \times (\vec{\xi}_\perp \times \vec{B})\,, \tag{10}$$

and

$$\delta\vec{E} = i\omega \vec{\xi} \times \vec{B} \ , \tag{11}$$

where $\delta\vec{E}$ is the perturbed electric field. The gyrokinetic description neglecting the Finite-Larmor-radius correction is employed for all particle species. $\delta\vec{\vec{p}}$ can be expressed as

$$\delta\vec{\vec{p}} = \delta p_{\perp} \vec{\vec{I}} + (\delta p_{||} - \delta p_{\perp}) \hat{b}\hat{b} \ , \tag{12}$$

where $\delta p_{||}$ and $\delta p_{\perp}$ are obtained from the perturbed particle distribution function δf by

$$\begin{pmatrix} \delta p_{||} \\ \delta p_{\perp} \end{pmatrix} = \sum_j M \int d^3v \, \delta f \begin{pmatrix} 2(\varepsilon - \mu B) \\ \mu B \end{pmatrix} \ , \tag{13}$$

where the summation in j is over all particle species, M is the particle mass, $\varepsilon = v^2/2$ is the particle energy, $\mu = v_{\perp}^2/2$ is the magnetic moment, and δf is the perturbed particle distribution function. In Eq. (13) the integral over velocity space can be expressed in terms of the new velocity space coordinates $(\varepsilon,\Lambda,\sigma)$

$$\int d^3v = \sum_{\sigma} \sqrt{2}\,\pi \int_0^{\infty} d\varepsilon\, \varepsilon^{1/2} \int_0^{h(\psi,\theta)} \frac{d\Lambda}{h\sqrt{1-\Lambda/h}} \ , \tag{14}$$

where the summation in σ is over the direction of particle parallel velocity, $\Lambda = \mu B_o/\varepsilon$ is the pitch angle, B_o is the vacuum magnetic field at X = R, and $h = B_o/B(\psi,\theta)$. On a flux surface, circulating particles correspond to $0 \le \Lambda \le h_{min}(\psi)$, and trapped particles to $h_{min}(\psi) \le \Lambda \le h$ at a given θ, where $h_{min}(\psi) = \text{Min}\,[h(\psi,\theta)]$ on the ψ surface. If we write δf as

$$\delta f = -\vec{\xi}_{\perp} \cdot \nabla F - \frac{\mu b_{||}}{B} \frac{\partial F}{\partial \mu} + \hat{g} \ , \tag{15}$$

where F is the unperturbed particle distribution, the nonadiabatic perturbed particle distribution is given by

$$\hat{g} = \int_{-\infty}^{t} dt' \left(-\frac{ieF}{T}\right)\left(\tilde{\omega} - \omega_*^T\right)\left[\frac{i\,\vec{v}_d \bullet \delta\vec{E}_\perp}{\omega} + \frac{M\mu b_\parallel}{e}\right] , \tag{16}$$

where the time integration is along the unperturbed particle characteristics, e is the particle charge, $b_\parallel$ is the parallel perturbed magnetic field, $\tilde{\omega} = -(T\omega/M)\partial \ln F/\partial\varepsilon$, $\omega_*^T = -i\,(T/M\omega_c)\,(\hat{b} \times \nabla \ln F \bullet \nabla)$ only operates on the perturbed quantities, $\vec{v}_d = (\hat{b}/\omega_c) \times [\,\nabla(\mu B) + \vec{\kappa}\, v_\parallel^2\,]$ is the magnetic drift velocity, $\hat{b} = \vec{B}/B$, T is the average temperature, ω_c is the cyclotron frequency.

In terms of the dependent variables, $\xi_\psi = \vec{\xi} \bullet \nabla\psi$, $b_\parallel = \vec{b} \bullet \vec{B}$, $\xi_s = \vec{\xi} \bullet (\vec{B} \times \nabla\psi / |\nabla\psi|^2)$, and $\nabla \bullet \vec{\xi}$, Eqs. (9) - (16) can be cast into a set of non-Hermitian integro-differential eigenmode equations which are solved by a nonvariational kinetic-MHD stability code (NOVA-K).[7] The NOVA-K code employs Fourier expansion in the poloidal angle θ direction, and cubic B-spline finite elements in the radial ψ direction. An arbitrary nonuniform ψ-mesh can be set up to provide the option of zoning the mesh to allow more finite elements near rational surfaces, the plasma edge, and the magnetic axis. The boundary condition at the magnetic axis is $\xi_\psi = 0$. For fixed boundary modes the boundary condition is $\xi_\psi = 0$ at the plasma-wall interface. In general, the boundary condition at the plasma-vacuum interface is given by $\vec{b}_v \bullet \nabla\psi = \vec{B} \bullet \nabla\xi_\psi$, where $\vec{b}_v$ is the perturbed vacuum magnetic field which must be solved from the divergence-free equation $\nabla \bullet \vec{b}_v = 0$ with proper wall boundary condition. In this paper, instead of presenting the full numerical solutions of the TAE instabilities from the NOVA-K code, we will consider a semi-analytical approach by establishing a quadratic dispersion relation and performing a perturbative analysis to obtain the stability criteria of the α-particle driven TAE modes.

III. Quadratic Form

By taking an inner product of Eq. (9) with $\vec{\xi}^*$ and integrating over all the plasma volume with the assumption of a fixed conducting boundary, we obtain from a quadratic form

$$D(\omega) = \delta W_f + \delta W_k - \delta K = 0 , \tag{17}$$

where the inertial energy is given by

$$\delta K = \omega^2 \int d^3x \, \rho \left|\vec{\xi}\right|^2 , \tag{18}$$

the fluid potential energy due to both the core and hot components is

$$\delta W_f = \int d^3x \left\{ \left|\vec{b}_\perp\right|^2 + \left|\nabla\bullet\vec{\xi}_\perp + 2\,\vec{\kappa}\bullet\vec{\xi}_\perp\right|^2 B^2 + \left(\frac{\vec{J}\bullet\vec{B}}{B^2}\right)\left(\vec{b}\times\vec{B}\right)\bullet\vec{\xi}_\perp^{\,*} - 2\left(\vec{\kappa}\bullet\vec{\xi}_\perp^{\,*}\right)\left(\vec{J}\times\vec{B}\right)\bullet\vec{\xi}_\perp \right\} , \tag{19}$$

and the kinetic potential energy due to all species is

$$\delta W_k = -\int d^3x \left\{ \nabla\bullet\vec{\xi}^{\,*}\ \delta\hat{p}_\perp + \left(\delta\hat{p}_\perp - \delta\hat{p}_\parallel\right)\left(\vec{\kappa}\bullet\vec{\xi}_\perp^{\,*} - \frac{\vec{B}\bullet\nabla\xi_\parallel^{\,*}}{B}\right)\right\} , \tag{20}$$

where the nonadiabatic perturbed pressures are defined by

$$\begin{pmatrix}\delta\hat{p}_\parallel \\ \delta\hat{p}_\perp\end{pmatrix} = \sum_j M\int d^3v\,\hat{g}\begin{pmatrix}2(\varepsilon-\mu B) \\ \mu B\end{pmatrix} . \tag{21}$$

The quadratic form is useful in providing the stability properties of the system in certain limits. A perturbative analysis can be performed over Eq. (17) to obtain the stability criteria of the TAE modes and is presented in Sec. IV. In terms of the Fourier components, the nonadiabatic trapped particle contribution to the potential energy neglecting the finite particle banana width effects can be written as

$$\delta W_k^t \approx -2^{7/2} M \pi^2 \int d\psi \int_0^{\infty} d\varepsilon\, \varepsilon^{5/2} \int_{h_{min}}^{h_{max}} d\Lambda\, K_b$$

$$\sum_{m',m,p} \left\langle G_{m',p}\, e^{iS_{m'}\theta} \right\rangle^* \frac{\left(\omega \frac{\partial F}{\partial \varepsilon} + \hat{\omega}_*^{(m)} F \right)}{\left(\omega - \langle \omega_d \rangle - p\, \omega_b \right)} \left\langle G_{m,p}\, e^{iS_m\theta} \right\rangle \quad , \tag{22}$$

where $G_{m,p} = \hat{G}_{m,p}[\cos^2(p\pi/2)\cos(p\omega_b \hat{t}) - i \sin^2(p\pi/2)\sin(p\omega_b \hat{t})]$, $\hat{G}_m(\Lambda,\psi,\theta)$ is defined by $[(1 - 3\Lambda/2h)\, \vec{\kappa} \cdot \vec{\xi}_\perp - (\Lambda/2h)\, \nabla \cdot \vec{\xi}_\perp] = \sum_m \hat{G}_m(\Lambda,\psi,\theta) \exp[i(m\theta - n\zeta)]$, $K_b = \sqrt{\varepsilon/2}\, \tau_b$, τ_b is the trapped particle bounce period and is a function of ε and Λ, $\hat{\omega}_*^{(m)} = (mM/eq)(\partial \ln F/\partial \psi)$, and $S_m = m - nq$, and $\langle A \rangle$ denotes the bounce or transit average of A and is given by

$$\langle A \rangle = \frac{1}{\tau_{b,t}} \oint \frac{A\, dl}{|v_{||}|} . \tag{23}$$

For trapped particles $\hat{t}(\theta)$ is defined by

$$\hat{t}(\theta, \sigma_{||} = +1) = \int_0^{\theta} \frac{J\, B\, d\theta'}{|v_{||}|} \quad , \tag{24}$$

where $\theta_T > \theta > -\theta_T$ corresponds to $(\tau_b/4) > \hat{t} > -(\tau_b/4)$, and $\pm\theta_T$ are the trapped particle turning points defined as the roots of the $v_{||}^2(\theta) \propto [1 - \Lambda/h(\theta)] = 0$.

Similarly, the nonadiabatic contributions of circulating particles on the potential energy is given by

$$\delta W_k^c \approx -2^{7/2} M \pi^2 \int d\psi \int_0^\infty d\varepsilon\, \varepsilon^{5/2} \int_0^{h_{min}} d\Lambda\, K_t \sum_{m,m',\tilde{p}=-\infty}^{\infty}$$

$$\left\langle \hat{G}_{m'} e^{i\left(S_{m'}\theta - S\tilde{p}\omega_t \hat{t}\right)} \right\rangle^* \frac{\left(\omega - \langle\omega_d\rangle\right)\left(\omega \frac{\partial F}{\partial \varepsilon} + \hat{\omega}_*^{(m)} F\right)}{\left(\omega - \langle\omega_d\rangle\right)^2 - \left(\tilde{p} - nq\right)^2 \omega_t^2} \left\langle \hat{G}_m e^{i\left(S_m\theta - S\tilde{p}\omega_t \hat{t}\right)} \right\rangle \quad (25)$$

where $K_t = \sqrt{2\varepsilon}\,\tau_t$, τ_t is the circulating particle transit period and is a function of ε and Λ. For circulating particles the time-like variable $\hat{t}(\theta)$ is defined by Eq. (24) but with $\pi > \theta > -\pi$ which corresponds to $(\tau_t/2) > \hat{t} > -(\tau_t/2)$.

V. Alpha-Particle Destabilization of the Toroidicity-Induced Alfven Eigenmodes

In this section, we will focus on the destabilization of shear Alfven waves by α-particles. For typical D-T parameters the α-particle birth velocity $V_\alpha = (2\varepsilon_\alpha/M_\alpha)^{1/2} = 1.295 \times 10^9$ cm/sec for an energy ε_α of 3.5 MeV is comparable to the Alfven speed $V_A = B/(N_i M_i)^{1/2}$. Thus, the transiting α-particles could destabilize shear Alfven waves by the expansion free energy associated with the spatial gradient of the α-particle pressure via inverse Landau damping through the $\omega = k_{||} v_{||}$ wave-particle resonance. Here, $k_{||} = (m\text{-}nq)/qR$ is the parallel wavenumber for linearized waves that are Fourier decomposed as $\exp[i(m\theta - n\zeta - \omega t)]$. To satisfy the resonance condition, it requires that $V_\alpha > V_A / 2\,|m\text{-}nq|$. To overcome the Landau damping by the inverse Landau damping associated with $\omega_{*\alpha}$, it requires roughly that $\omega_{*\alpha} > \omega_A = V_A/qR$.

The stability of a global Alfven wave due to wave-particle resonances can be obtained perturbatively from the quadratic form, Eq. (17). We write the mode frequency as $\omega = \omega_r + i\gamma$ and assume that the growth rate is small ($|\gamma| << |\omega_r|$). Then we have

$$\omega_r^2 \approx \{\, \delta W_f + \mathrm{Prin}\,[\delta W_k]\,\} / \delta K\,, \quad (26)$$

and

$$\gamma \approx \mathrm{Res}\,[\delta W_k] / 2\, i\, \omega_r \delta K, \quad (27)$$

where Prin $[\delta W_k]$ and Res $[\delta W_k]$ are the principal part and resonance contribution, respectively. The wave particle resonances due to all particle species are retained in Res $[\delta W_k]$. The core electron and ion distributions are taken as Maxwellians. The α-particle equilibrium distribution function, F_α, was taken to be isotropic in pitch angle variable Λ and slowing-down in energy for $\varepsilon \leq \varepsilon_\alpha$ and zero for $\varepsilon > \varepsilon_\alpha$. The tokamak reactor type equilibria are modeled with noncircular plasma surfaces defined by

$$X = R + a\cos[\theta + \delta\sin(\theta)] , \tag{28}$$

and

$$Z = \kappa a \sin(\theta) , \tag{29}$$

where κ is the elliticity, δ is the triangularity, a is the horizontal minor radius, and R is the major radius. The equilibrium pressure and safety profiles are chosen as

$$P(y) = P_o\left(1-y^\lambda\right)^\mu , \tag{30}$$

$$q(y) = q(0) + y\left\{q(1) - q(0) + \left[q'(1) - q(1) + q(0)\right]\frac{(1-y_s)(y-1)}{(y-y_s)}\right\} , \tag{31}$$

where $y_s = [q'(1) - q(1) + q(0)]/\{q'(0) + q'(1) - 2[q(1) - q(0)]\}$, $y = (r/a)^2 = (\psi - \psi_o)/\Delta\psi$, $\Delta\psi = \psi_{lim} - \psi_o$, ψ_{lim} is evaluated at the limiter, and ψ_o is evaluated at the magnetic axis.

The lowest order solutions, determined by Eq. (25), must be obtained from the solutions of the appropriate eigenmode equations, Eqs. (9) - (15), by neglecting the resonance contributions to the perturbed particle pressures. If the nonadiabatic perturbed pressures defined in Eq. (21) can also be neglected, i.e., the Prin $[\delta W_k]$ contribution is neglected, the eigenmode equations, Eqs. (9) - (15), correspond to the ideal MHD equations in the limit of vanishing ratio of specific heat, and can be readily solved by the NOVA code.[10] In the following we will adopt this approximation in calculating the lowest order solutions of the TAE modes and greatly reduce the amount of numerical computations. Physically this approximation eliminates the ion sound waves. The more complete lowest order solutions will be carried out in the future works.

A. Existence of the Toroidicity-Induced Eigenmode

Briefly, let us describe the various types of shear Alfven waves in a tokamak plasma. The ideal MHD equation of motion shows that the coefficient of the highest-order radial derivative term, $d^2\xi_r/dr^2$, where ξ_r is the radial fluid displacement, vanishes at radial locations where $\omega^2 = (k_{||}V_A)^2$. This corresponds to the shear Alfven resonance condition, and frequencies ω that satisfy $\min[(k_{||}V_A)^2] < \omega^2 < \max[(k_{||}V_A)^2]$ lie in the shear Alfven continuum. This resonance leads to a singular mode structure; however, if electron parallel dynamics and ion finite Larmor radius effects are included, one obtains a nonsingular solution known as the kinetic Alfven wave (KAW). Its mode structure is fairly localized, and hence it is stable to α-particle drive due to strong electron Landau damping.[11]

There are two global types of shear Alfven waves that have radially extended mode structure. Both types have low mode numbers n and m. The first type of global shear Alfven wave is a regular, spatially nonresonant wave whose frequency lies just below the minimum of the continuum, i.e., $\omega < k_{||}V_A$ and $k_{||} \neq 0$. This wave is called the Global Alfven Eigenmode (GAE).[12] Previous theoretical analysis of this mode was limited to cylindrical geometry, where it was found that transit wave-particle resonant interaction with super-Alfvenic α-particles could destabilize it, although with weak growth rates.[11] When finite toroidicity is included, GAE modes with different poloidal mode numbers will become coupled. Such toroidal mode coupling tends to stabilize the GAE modes completely.[3,8]

Another type of global shear Alfven wave, one that exists only in toroidal geometry. The existence of this so-called Toroidicity-Induced Alfven Eigenmode (TAE) was shown in the ideal MHD limit without α-particles.[1,13,14] Finite toroidicity introduces the TAE mode, which can be strongly destabilized by α-particles. The TAE mode exists inside gaps, due to toroidal coupling, in the shear Alfven continuum spectrum. For example, modes (n,m) and (n,m+1) couple at radial location r_o, where $q(r_o) = (m + 1/2)/n$, to form a gap which is bounded by

$$\omega_{\pm}^2 = \omega_o^2 \pm 2\,\omega_o^2 \left(\frac{r_o}{R} + \Delta'(r_o)\right) , \tag{32}$$

where the center of the continuum gap is $\omega_o^2 = (V_A/2qR)^2$ at $r = r_o$, $\Delta(r)$ is the Shafranov shift of the nonconcentric flux surfaces and $\Delta' > 0$. For a given toroidal mode number n, the gaps due to the poloidal harmonic couplings can exist across the minor radius and form a frequency gap in the Alfven continuous spectrum. In this case the discrete global TAE modes had been shown to exist

with frequency inside the continuum gap.[1] The existence of the high-n TAE modes has also been shown previously.[13,14] Figure 1 shows the continuous spectrum in the absence of dissipations for the n=1 mode as a function of the radius for a circular TFTR equilibrium (ETFTR1). The parameters for the pressure and q-profiles of the "ETFTR1" equilibrium are P_o= 0.6, λ = 1.05, μ = 2, q(0) = 1.01, q(1) = 3.1, q'(0) = 0.84375, and q'(1) = 6.8571, $\beta = 2\langle P\rangle/\langle B^2\rangle$ = 1.2223%, β_{pol} = 0.8924. Since TFTR will be operated in the super shot regime with peak density profiles, the density profiles is taken to be $\rho(y) = \rho(0)\,(1 - 0.8\,y)$. The minor radius is a= 0.8, and the major radius is R = 2.5. The frequency of the n=1 fixed boundary TAE mode is given by $(\omega/\omega_A)^2$ = 0.7656, which lies within the continuum gap, $0.7 \geq (\omega/\omega_A)^2 \geq 3.2$, formed by the toroidal coupling of the m=1, 2, and 3 poloidal harmonics at q=1.5 and 2.5 surfaces. The normalized Alfven frequency is defined as $\omega_A = v_A(0) / q(1)R$. The eigenfunction ξ_ψ of the n=1 fixed boundary TAE mode versus r/a is shown in terms of poloidal harmonics in Fig. 2, which clearly shows the dominant m=1 and 2 components peaking near the q=1.5 surface.

Since ω_0^2 is roughly proportional to $(1/q^2\rho)$, for certain q and density profiles it can vary radially so that the continuum frequency gap does not exist for all minor radius. For higher n modes (n > 2), it is less possible for a frequency gap to exist. Typically the higher poloidal harmonic of the TAE mode will resonate with the Alfven continuum near the plasma edge and suffer damping (electron Landau damping) as in the case of kinetic Alfven waves. The total electron damping rate of the TAE mode can be roughly estimated as[6,15]

$$\gamma_e / \omega_A \approx \beta_e\,(v_A/v_e) / 2(k_{||}R)^2 + \pi^{1/2}\,(k_\perp\rho_s)^2\,(v_A/v_e)\,A_m^2\,W_m\,, \qquad (33)$$

where ρ_s is the ion gyroradius with the electron temperature, v_e is the electron thermal velocity, A_m is the relative amplitude of the resonant higher-m harmonic to that of the nonresonant lower-m poloidal harmonics and is estimated to be (a/R), W_m is the ratio of the resonant poloidal mode localization width to the nonresonant poloidal mode localization width and is estimated to be $1/k_\perp a$. The first term in Eq. (33) is due to the electron Landau damping associated with the magnetic drift for the global m=1 and 2 harmonics contributed mainly from near q=1.5 surface. The second term is related to the electron parallel dynamics and ion finite Larmor radius effects associated with the localized kinetic Alfven wave of higher poloidal harmonics near its resonance surface. The continuum resonant damping rate is roughly a factor of $k_\perp a\rho_s^2/R^2\beta_e$ smaller compared with the nonresonant electron damping rate. More accurate numerical investigation of the resonant damping effect on the TAE mode is underway and will be presented in the future works.

B. Local Stability Analysis

If the particle trapping effects and the magnetic drift term in the resonance are ignored, the local instability criterion of the TAE mode for a low-β, large aspect ratio tokamak equilibrium can be obtained analytically by integrating over the velocity space in Res $[\delta W_k]$. At a radial position with the resonance condition $v_{||} = \omega / k_{||} = v_p$ and for a poloidal harmonic, Res $[\delta W_k] = g(\psi,m)$ $I(\psi,m)$ for each species, where $g(\psi,m)$ represents the mode amplitude weighting and is independent of particle species, and $I(\psi,m)$ represents the velocity integration and is given by

$$I(\psi,m) = \int dv_{||} dv_{\perp}^2 \left(M \omega \omega \frac{\partial F}{\partial \varepsilon} + \hat{\omega}_*^{(m)} F \right) \left(v_{\perp}^2 + 2 v_{||}^2 \right)^2 \delta(v_{||}^2 - v_p^2) \, . \tag{34}$$

For α-particle we have

$$I_\alpha(\psi,m) = \frac{3 P_\alpha \omega}{2\pi v_p v_\alpha} \left\{ \omega \left[\frac{4\hat{v}_p}{\hat{v}_\alpha} + \frac{3 - 4\hat{v}_p^2}{\hat{v}_\alpha (1 + \hat{v}_p^2)^{3/2}} + \frac{(v_\alpha^2 + v_p^2)^2}{v_\alpha^4} \right] \right.$$

$$\left. - \left(\frac{2 \omega_{*\alpha}^{(m)}}{3 \hat{v}_\alpha^3} \right) \left[\frac{1 + 8\hat{v}_p^2 + 4\hat{v}_p^4}{(1 + \hat{v}_p^2)^{1/2}} - 4\hat{v}_p^3 \right] \right\} \, , \tag{35}$$

where $\hat{v}_\alpha^2 = v_\alpha^2 / [v_\alpha^2 - v_p^2]$, $\hat{v}_p^2 = v_p^2 / [v_\alpha^2 - v_p^2]$, v_α is the alpha birth velocity, $\omega_{*\alpha}^{(m)} = m \rho_\alpha v_\alpha / 2r\tilde{L}_\alpha$, ρ_α is the alpha particle gyroradius at birth velocity, r is the minor radius, and $\tilde{L}_\alpha$ is the alpha particle pressure scale length. For the core electrons and ions we get

$$I_c(\psi,m) \approx \sum_j \left(4 \omega^2 P_j / \pi^{3/2} v_p v_j \right) \left[1 + 2 z_j^2 + 2 z_j^4 \right] \exp(-z_j^2) \, , \tag{36}$$

where the summation index j is over the electron and core ion species, $v_j = (2T_j / m_j)^{1/2}$, $z_j = v_p / v_j$. Evaluated at the q=1.5 surface with $v_p = v_A$ and $\omega = v_A / 2qR$, the instability condition is given by

$$\beta_\alpha \left\{ \frac{4\,\omega_{*\alpha}^{(m)}}{3\,\omega_A \hat{v}_\alpha^2} \left[\frac{(1+8\hat{v}_A^2+4\hat{v}_A^4)}{(1+\hat{v}_A^2)^{1/2}} - 4\hat{v}_A^3 \right] - \left[4\hat{v}_A + \frac{(3-4\hat{v}_A^2)}{(1+\hat{v}_A^2)^{3/2}} + \frac{\hat{v}_\alpha (v_\alpha^2+v_A^2)^2}{v_\alpha^4} \right] \right\}$$

$$\geq [8\, v_\alpha \hat{v}_\alpha / 3\pi^{1/2} v_A] \sum_j \beta_j z_j [1 + 2z_j^2 + 2z_j^4] \exp(-z_j^2). \qquad (37)$$

The first term on the left hand side is due to the α-particle destabilizing inverse Landau damping associated with its pressure gradient and the second term is associated with the α-particle velocity Landau damping. The right-hand side contribution is due to the stabilizing electron and core ion Landau dampings. Note that $\beta_j z_j$ are not free parameters and are proportional to (v_α/v_A). Equation (37) shows that to destabilize the TAE mode the α-particle free energy drive associated with $\omega_{*\alpha}$ must be large enough to overcome the usual Landau damping (typically when $\omega_{*\alpha}/\omega_A > 1$) and that above this threshold the growth rate γ will scale linearly with $\omega_{*\alpha}$.

The critical β_α vs. (v_α/v_A) stability curves computed from Eq. (37) are shown in Fig. 3 with m=2 for the TFTR, CIT, and ITER D-T operation parameters with very small critical β_α. The minimum critical β_α occurs at $v_\alpha/v_A \approx \sqrt{2}$, where the instability condition is roughly given by $\beta_\alpha(\omega_{*\alpha}/\omega_A - 2) \geq 0.4\,(M_e v_e / M_i v_\alpha)$. For $v_\alpha/v_A > 4$ the ion Landau damping becomes important. For TFTR the D-T operation parameters are chosen as R = 250 cm, a = 80 cm, B = 5 T, T_e = 10 kev, T_i = 10 kev, $\tilde{L}_\alpha$ = 15 cm, r = 25 cm, the alpha charge state Z_α = 2, M_α / M_p = 4, M_i / M_p = 2.5, where M_p, M_i, and M_α are the proton, core ion, and alpha masses, respectively. For n_i = 10^{14} cm^{-3}, we have v_α/v_A = 1.88 and the critical $\beta_\alpha = 2.5 \times 10^{-4}$. For CIT the parameters are chosen as R = 210 cm, a = 65 cm, B = 11 T, T_e = 10 kev, T_i = 10 kev, $\tilde{L}_\alpha$ = 20 cm, r = 16 cm, and the critical $\beta_\alpha = 7.5 \times 10^{-4}$ for v_α/v_A = 1.5. For ITER the parameters are chosen as R = 600 cm, a = 215 cm, B = 4.85 T, T_e = 10 kev, T_i = 10 kev, $\tilde{L}_\alpha$ = 50 cm, r = 50 cm, and the critical $\beta_\alpha = 1.2 \times 10^{-3}$ for v_α/v_A = 1.5. Note that we have chosen a steeper α-particle pressure gradient for TFTR to simulate the super shot operations so that its critical β_α is smaller.

C. Global Stability Analysis

A more complete nonlocal perturbative stability calculation can be performed for realistic equilibria by first obtaining the zeroth order solutions (eigenfuntions and mode frequency) from the NOVA code. Then the proper weightings due to the equilibrium profiles and the poloidal and radial

structures of the eigenfunctions in Res[δW_k] required to compute the growth rate from Eq. (27) can be integrated. Typically $<\omega_d>$ is much smaller than ω_t and ω_b and can be neglected except at the boundary between circulating and trapped particles, where $<\omega_d>$ has a logarithmic singularity and both ω_t and ω_b vanish. For larger minor radius, ω_t decreases and ω_b increases, but ω_t is about a factor of 2 to 4 larger than ω_b. Thus, for typical reactor parameters the α-particle transit resonances can more effectively destabilize the TAE mode than the bounces resonances. In the numerical computation of Res[δW_k] we have summed up many transit and bounce resonance terms to ensure its convergence. We also assume the α-particle density to be $n_\alpha = n_\alpha(0) \exp [- (r / L_\alpha)^2]$, and the volume averaged α-particle beta $<\beta_\alpha>$ is related to the central α-particle beta $\beta_\alpha(0)$ by $<\beta_\alpha> = (a / L_\alpha)^2 \beta_\alpha(0)$. The α-particle density scale length is $L_\alpha^2 / 2r$.

For TFTR we will study the circular tokamak equilibrium described in Fig. 1. The real frequency of the n=1 fixed boundary TAE mode is $\omega_r/\omega_A = - 0.875$. The corresponding eigenfunction ξ_ψ of the n=1 fixed boundary TAE mode versus r/a is shown in terms of poloidal harmonics in Fig. 2. The critical volume averaged $<\beta_\alpha>$ vs. (v_α/v_A) stability curves obtained from Eq. (27) are shown in Fig. 4 for the TFTR D-T parameters T_{eo} = 10 keV, T_{io} = 30 keV, R = 250 cm, a = 80 cm, B_o = 5 T, but with several L_α/a values. The electrons and the ions are assumed to have the same temperature profiles. The very small critical volume averaged α-particle beta $<\beta_\alpha>$ is consistent with the local stability calculations when the volume average of the alpha density is taken into account. For $v_\alpha/v_A = 1$ and $L_\alpha/a = 0.3$, the critical $<\beta_\alpha> = 1.5 \times 10^{-4}$.

Similar calculations are performed for the CIT and ITER parameters. For CIT we will study a noncircular tokamak equilibrium (ECIT2) with the following fixed parameters: R = 2.1, a = 0.65, κ = 2, δ = 0.2, P_o = 0.6, λ = 1.05, μ = 2, q(0) = 1.01, q(1) = 3.1, q'(0) = 0.9, q'(1) = 13. The plasma beta $\beta = 2<P>/<B^2> = 2.206\%$, and $\beta_{pol} = 0.639$. The plasma density is assumed to be constant. The real frequency of the n=1 fixed boundary TAE mode is $\omega_r/\omega_A = - 0.82$. The corresponding eigenfunction ξ_ψ of the n=1 fixed boundary TAE mode versus r/a is shown in terms of poloidal harmonics in Fig. 5, which clearly shows the dominant m=1 and 2 components. The critical volume averaged α-particle beta $<\beta_\alpha>$ vs. (v_α/v_A) stability curves are shown in Fig. 6 for the CIT physical parameters $T_{eo} = T_{io}$ = 10 keV, R = 210 cm, a = 65 cm, B_o = 11 T, but with several L_α/a values. The electrons and the ions are assumed to have the same temperature profiles. The very small critical $<\beta_\alpha>$ is consistent with the local stability calculations when the volume average of the alpha density is taken into account. For $v_\alpha/v_A = 1.3$, and $L_\alpha/a = 0.2$, the critical $<\beta_\alpha> = 8 \times 10^{-6}$. Higher ion temperature provides higher ion Landau damping, and the critical $<\beta_\alpha>$ vs. (v_α/v_A) stability curves for $T_{eo} = T_{io}$ = 20 keV are about a factor of three higher than

those for $T_{eo} = T_{io} = 10$ keV. As the α-particle pressure sacle length increases, the TAE mode will be stable. For $T_{eo} = T_{io} = 10$ keV case, the TAE mode is stable for $L_\alpha/a > 0.4$.

For ITER we will study a noncircular tokamak equilibrium (EITER1) with the following fixed parameters: R = 6, a = 2.15, $\kappa = 2$, $\delta = 0.4$, $P_0 = 1$, $\lambda = 1.05$, $\mu = 2$, q(0) = 1.01, q(1) = 3.2, q'(0) = 0.9, q'(1) = 13. This equilibrium is similar to the "ECIT2" equilibrium employed for CIT but with its triangularity being twice as large. The total plasma beta $\beta = 2\langle P\rangle/\langle B^2\rangle = 2.17\%$, and $\beta_{pol} = 0.474$. The plasma density is assumed to be constant. The real frequency of the n=1 fixed boundary TAE mode is $\omega_r/\omega_A = -0.857$. The corresponding eigenfunction ξ_ψ of the n=1 fixed boundary TAE mode versus r/a is shown in terms of poloidal harmonics in Fig. 7, which are quite similar to those of the "ECIT2" equilibrium shown in Fig. 5. The critical $\langle\beta_\alpha\rangle$ vs. (v_α/v_A) stability curves are shown in Fig. 8 for the ITER physical parameters $T_{eo} = T_{io} = 10$ keV, R = 600 cm, a = 215 cm, $B_0 = 4.85$ T, but with several L_α/a values. The electrons and the ions have the same temperature profiles. The critical $\langle\beta_\alpha\rangle$ is roughly a factor of three higher than that of CIT case shown in Fig. 6, which is due to the larger ion Landau damping. For $v_\alpha/v_A = 1.3$, and $L_\alpha/a = 0.2$, the critical $\langle\beta_\alpha\rangle = 2.2 \times 10^{-5}$. Calculations are also performed for higher electron and ion temperatures, and the results shown in Fig. 8 for $T_{eo} = T_{io} = 20$ keV are similar to those obtained for CIT case.

From these results we find that for typical D-T tokamak parameters, the volume averaged α-particle beta threshold for TAE instability is very small and is in the order of 10^{-4}. The TAE modes will be robustly unstable in these proposed D-T tokamaks with typical growth rates in the order of $10^{-2}\omega_A$ as shown previously.[2,3]

V. Summary and Conclusion

In the paper we have studied the stability property of the α-particle driven toroidicity-induced shear Alfven eigenmodes (TAE) via inverse Landau damping associated with the spatial gradient of the α-particle pressure. In determining the volume averaged α-particle beta threshold for TAE instability, we have included the core ion and electron kinetic effects. A quadratic dispersion relation is derived and a perturbative analysis is performed to obtain the α-particle beta threshold with the aid of the NOVA-K code. For D-T tokamaks the TAE modes can be strongly unstable with the growth rate being approximately linearly proportional to $\omega_{*\alpha}$ and typically of the

order of $10^{-2}\ \omega_A$. Other types of global Alfven waves had been shown to be stable in D-T tokamaks due to toroidal coupling effects. Therefore, primary attention - especially experimental - should be focused on the TAE modes, which can be strongly destabilized by α-particles.

The nonlinear behavior of the α-particle driven TAE modes is recently investigated[16] with a model in which the finite amplitude of the TAE mode alters the α-particle interaction with the mode. The α-particle distribution is flattened locally in phase space by the perturbed magnetic field which reduces the α-particle-to-wave energy transfer rate below the ambient dissipation rate. Rough estimates yield a saturation level given by $\delta B_r/B \approx 5 \times 10^{-5} (\beta_\alpha/\beta_{\alpha crit})^{2/3}$. From our calculations presented in the paper we have $\beta_\alpha/\beta_{\alpha crit} \approx 10^2 - 10^3$ for typical D-T tokamaks, and the saturation level of the TAE mode will be $\delta B_r/B \approx 10^{-3}$. At this level of the magnetic fluctuation the α-particle loss time will be appreciably shorter than the α-particle slowing-down time.[9] A more complete calculation of the TAE mode saturation level with self-consistent eigenfunctions will be addressed in the future works.

Experimental efforts in TFTR are now underway to excite the TAE mode by neutral beam injection. Since the TAE modes is predicted to be weakly damped and therefore high-Q, a less expensive way to excite the TAE modes is by low power antennas whose impedance will have sharp spikes of the TAE eigenfrequencies.[17] The eigenmode structure can be measured by poloidal and toroidal magnetic probes and compared with the theory.

Finally, we believe that the theoretical studies of the linear TAE mode stability presented in the work can still be improved. Some important α-particle particle physics that should be addressed in the future are finite banana width, finite Larmor radius, and more realistic α-particle distribution functions generated from Fokker-Planck code. Core ion kinetic effects such as finite Larmor radius and pressure anisotropy can be also important. The stabilizing electron Landau damping effects associated with the parallel electric field must be addressed if the TAE mode frequency runs into the continuous spectrum of the higher poloidal harmonics.

ACKNOWLEDGMENTS

The authors would like to thank Drs. G. Y. Fu, H. L. Berk, D. J. Sigmar, J. W. Van Dam, and S. J. Zweben for useful discussions. This work was supported by U.S. Department of Energy Contract No. DE-AC02-76-CHO-3073.

REFERENCES

1. C. Z. Cheng and M.S. Chance, Phys. Fluids **29**, 3695 (1986).
2. C. Z. Cheng, Phys. Fluids B **2**, 1427 (1990).
3. C. Z. Cheng, G. Y. Fu, and J. W. Van Dam, in Proceedings of Workshop on Theory of Fusion Plasmas, Chexbres, Swizerland, 1988 (ed. J. Vaclavik, F. Troyon, and E. Sindoni, Societa Italiana di Fisica, Bologna, 1989), p. 259.
4. G. Y. Fu and J. W. Van Dam, Phys. Fluids B **1**, 1949 (1989).
5. C. Z. Cheng, to be published in Fusion Technology (1990).
6. J. W. Van Dam, G. Y. Fu, and C. Z. Cheng, The University of Texas Report, IFSR-413 (January, 1990), to be published in Fusion Technology (1990).
7. C. Z. Cheng, Princeton Plasma Physics Laboratory Report, PPPL-2604 (April, 1989), to be published in Computer Physics Report.
8. G. Y. Fu and J. W. Van Dam, Phys. Fluids B **1**, 2404 (1989).
9. D. J. Sigmar, C. T. Hsu, R. B. White, and C. Z. Cheng, MIT Report, PFC/JA-89-58 (1989).
10. C. Z. Cheng and M. S. Chance, J. Comput. Phys. **71**, 124 (1987).
11. Y. M. Li, S. M. Mahajan, and D. W. Ross, Phys. Fluids **30**, 1466 (1987).
12. K. Appert, R. Gruber, F. Troyon, and J. Vaclavik, Plasma Physics **24**, 1147 (1982); S. M. Mahajan, D. W. Ross, and G. L. Chen, Phys. Fluids **26**, 2195 (1983).
13. C. Z. Cheng, L. Chen and M. S. Chance, Ann. Phys. (NY) **161**, 21 (1985).
14. G. Y. Fu and C. Z. Cheng, Phys. Fluids B **2**, 985 (1990).
15. K. T. Tsang, D. J. Sigmar, and J. C. Whitson, Phys. Fluids **24**, 1508 (1981).
16. H. L. Berk and B. N. Breizman, The University of Texas Report, IFSR-396 (September, 1989), to be published in Phys. Fluids (1990).
17. R. E. Stockdale and C. Z. Cheng, Bull. Am. Phys. Soc. **30**, 1592 (1985).

Figure Captions

Fig. 1 The Alfven continuous spectrum of a circular TFTR equilibrium "ETFTR1" with the minor radius a = 0.8, and the major radius R = 2.5. The total pressure and q-profiles are given by Eqs. (30) and (31) with $P_o = 0.6$, $\lambda = 1.05$, $\mu = 2$, $q(0) = 1.01$, $q(1) = 3.1$, $q'(0) = 0.84375$, $q'(1) = 6.8571$, $\beta = 1.2223\%$, and $\beta_{pol} = 0.8924$..

Fig.2 The poloidal harmonics of eigenfunction ξ_ψ of the n=1 fixed boundary toroidicity-induced Alfven eigenmode (TAE) versus r/a for the "ETFTR1" equilibrium. The real frequency of the n=1 fixed boundary TAE mode is $\omega_r/\omega_A = - 0.875$.

Fig. 3 The critical β_α vs. (v_α/v_A) stability curves for the toroidicity-induced Alfven eigenmode (TAE) computed from Eq. (37) with m=2 for the TFTR, CIT, and ITER D-T operation parameters.

Fig. 4 The critical volume averaged $<\beta_\alpha>$ vs. (v_α/v_A) stability curves for the "ETFTR1" equilibrium with the D-T parameters $T_{eo} = 10$ keV, $T_{io} = 30$ keV, R = 250 cm, a = 80 cm, and $B_o = 5$ T, but with several L_α/a values.

Fig.5 The poloidal harmonics of eigenfunction ξ_ψ of the n=1 fixed boundary toroidicity-induced Alfven eigenmode (TAE) versus r/a for the "ECIT2" equilibrium. The equilibrium is defined by the parameters: R = 2.1, a = 0.65, $\kappa = 2$, $\delta = 0.2$, $P_0 = 0.6$, $\lambda = 1.05$, $\mu = 2$, $q(0) = 1.01$, $q(1) = 3.1$, $q'(0) = 0.9$, $q'(1) = 13$. The plasma beta $\beta = 2<P>/<B^2> = 2.206\%$, and $\beta_{pol} = 0.639$. The plasma density is assumed to be constant. The real frequency of the n=1 fixed boundary TAE mode is $\omega_r/\omega_A = - 0.82$.

Fig. 6 The critical volume averaged α-particle beta $<\beta_\alpha>$ vs. (v_α/v_A) stability curves for the "ECIT2" equilibrium with the physical parameters $T_{eo} = T_{io} = 10$ keV, R = 210 cm, a = 65 cm, $B_o = 11$ T, but with several L_α/a values. The electrons and the ions are assumed to have the same temperature profiles. Higher ion temperature provides higher ion Landau damping, and the critical $<\beta_\alpha>$ vs. (v_α/v_A) stability curves for $T_{eo} = T_{io} = 20$ keV are about a factor of three higher than those for $T_{eo} = T_{io} = 10$ keV.

Fig. 7 The poloidal harmonics of eigenfunction ξ_ψ of the n=1 fixed boundary toroidicity-induced Alfven eigenmode (TAE) versus r/a for the "EITER1" equilibrium. The equilibrium is defined by

the parameters: R = 6, a = 2.15, κ = 2, δ = 0.4, P_o = 1, λ = 1.05, μ = 2, q(0) = 1.01, q(1) = 3.2, q'(0) = 0.9, q'(1) = 13.. The plasma beta $\beta = 2\langle P\rangle/\langle B^2\rangle$ = 2.17%, and β_{pol} = 0.474. The plasma density is assumed to be constant. The real frequency of the n=1 fixed boundary TAE mode is ω_r/ω_A = - 0.857.

Fig. 8 The critical $\langle\beta_\alpha\rangle$ vs. (v_α/v_A) stability curves for the ITER physical parameters $T_{eo} = T_{io}$ = 10 keV, R = 600 cm, a = 215 cm, B_o = 4.85 T, but with several L_α/a values. The cases with T_{eo} = T_{io} = 20 keV are also shown.

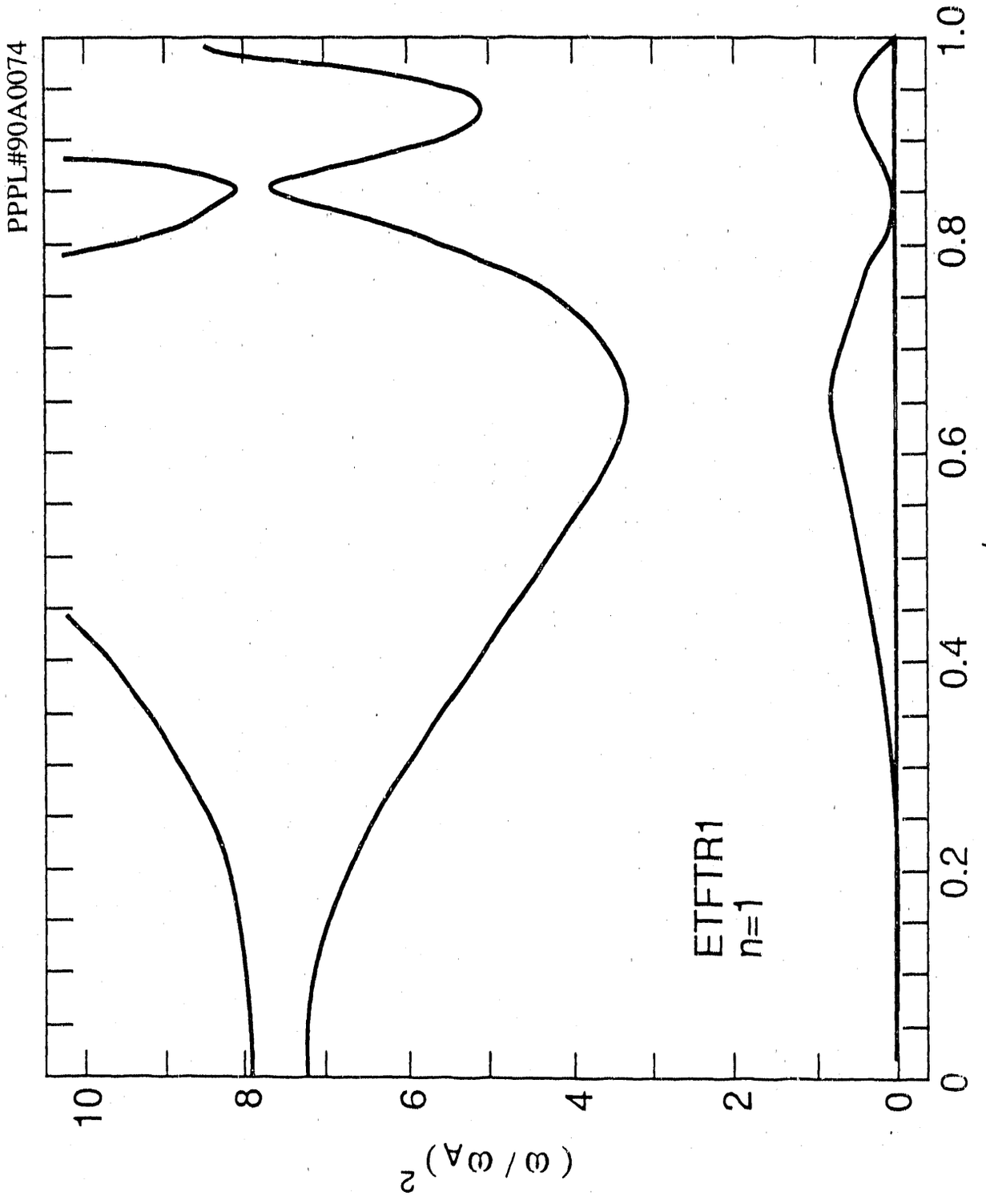
PPPL#90A0074
ETFTR1
n=1
$(\omega / \omega_A)^2$
r / a
0
2
4
6
8
10
0
0.2
0.4
0.6
0.8
1.0

Figure 1

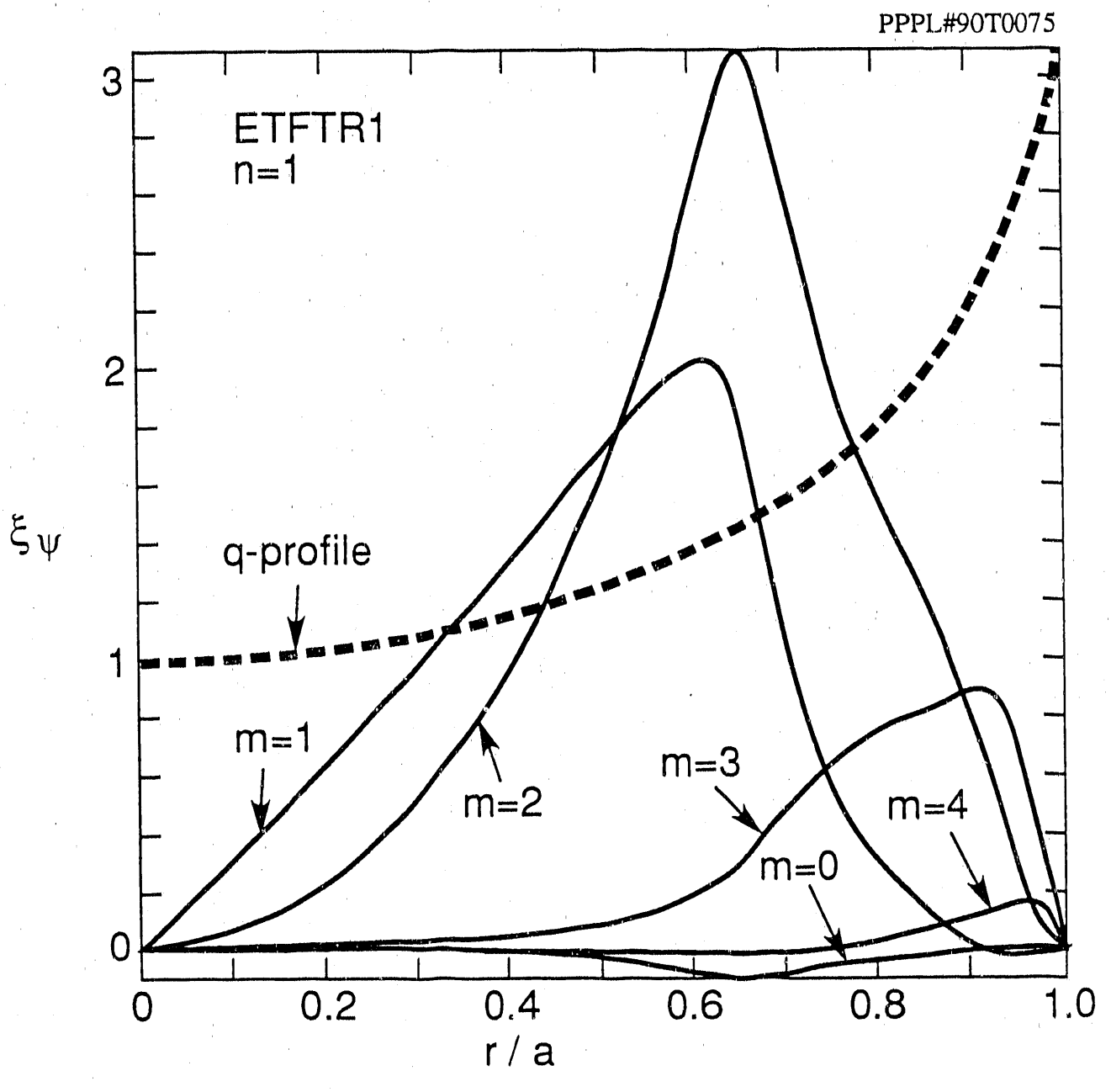
PPPL#90T0075
ETFTR1
n=1
q-profile
m=1
m=2
m=3
m=0
m=4
ξ_ψ
r / a
0
0.2
0.4
0.6
0.8
1.0
1
2
3

Figure 2

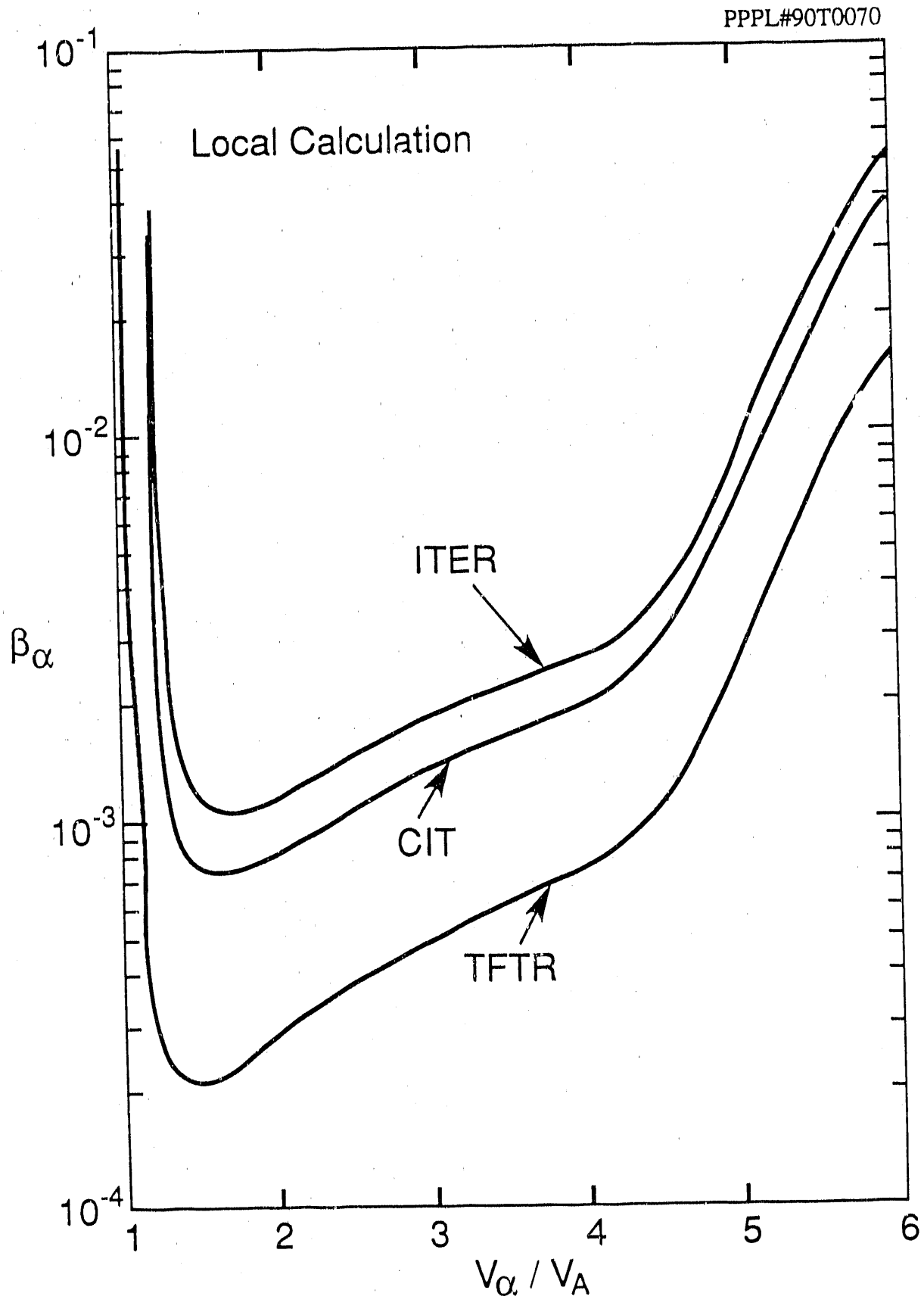
PPPL#90T0070
Local Calculation
ITER
CIT
TFTR
β_α
V_α / V_A
10^{-1}
10^{-2}
10^{-3}
10^{-4}
1
2
3
4
5
6

Figure 3

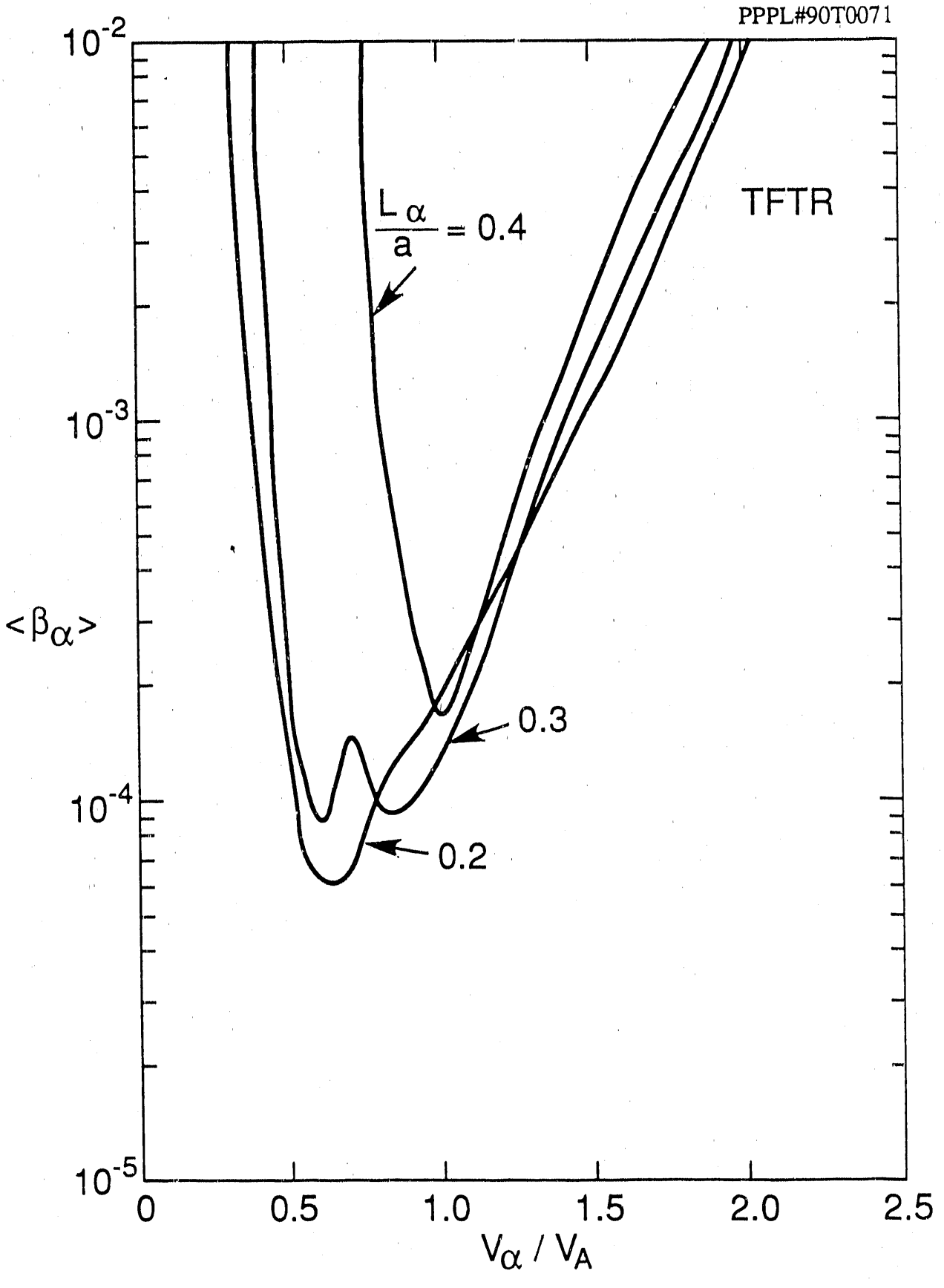
PPPL#90T0071
TFTR
$\frac{L\alpha}{a} = 0.4$
0.3
0.2
10^{-2}
10^{-3}
10^{-4}
10^{-5}
$<\beta_\alpha>$
0
0.5
1.0
1.5
2.0
2.5
V_α / V_A

Figure 4

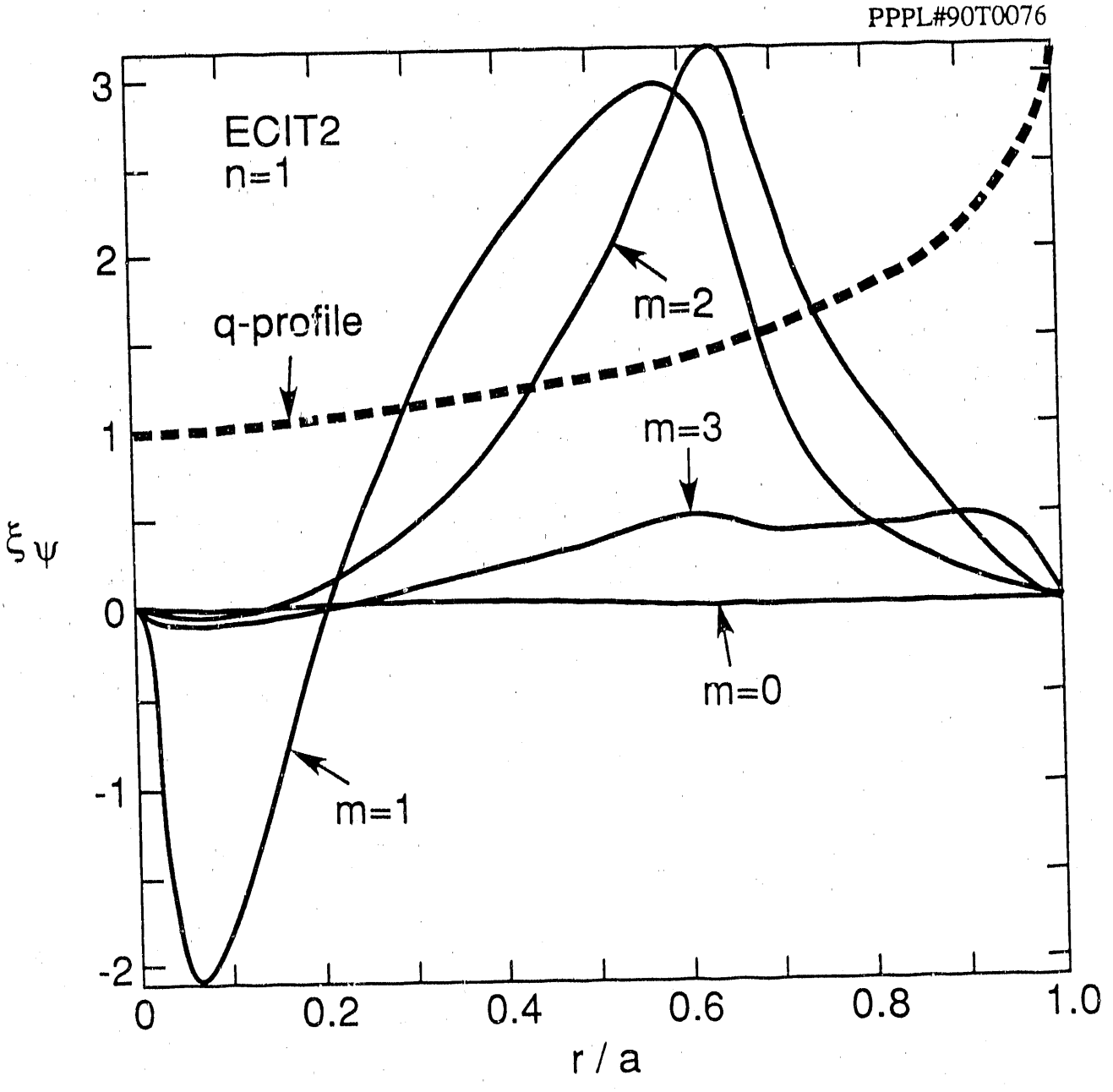
PPPL#90T0076
ECIT2
n=1
q-profile
m=2
m=3
m=0
m=1
ξ_ψ
3
2
1
0
-1
-2
0
0.2
0.4
0.6
0.8
1.0
r / a

Figure 5

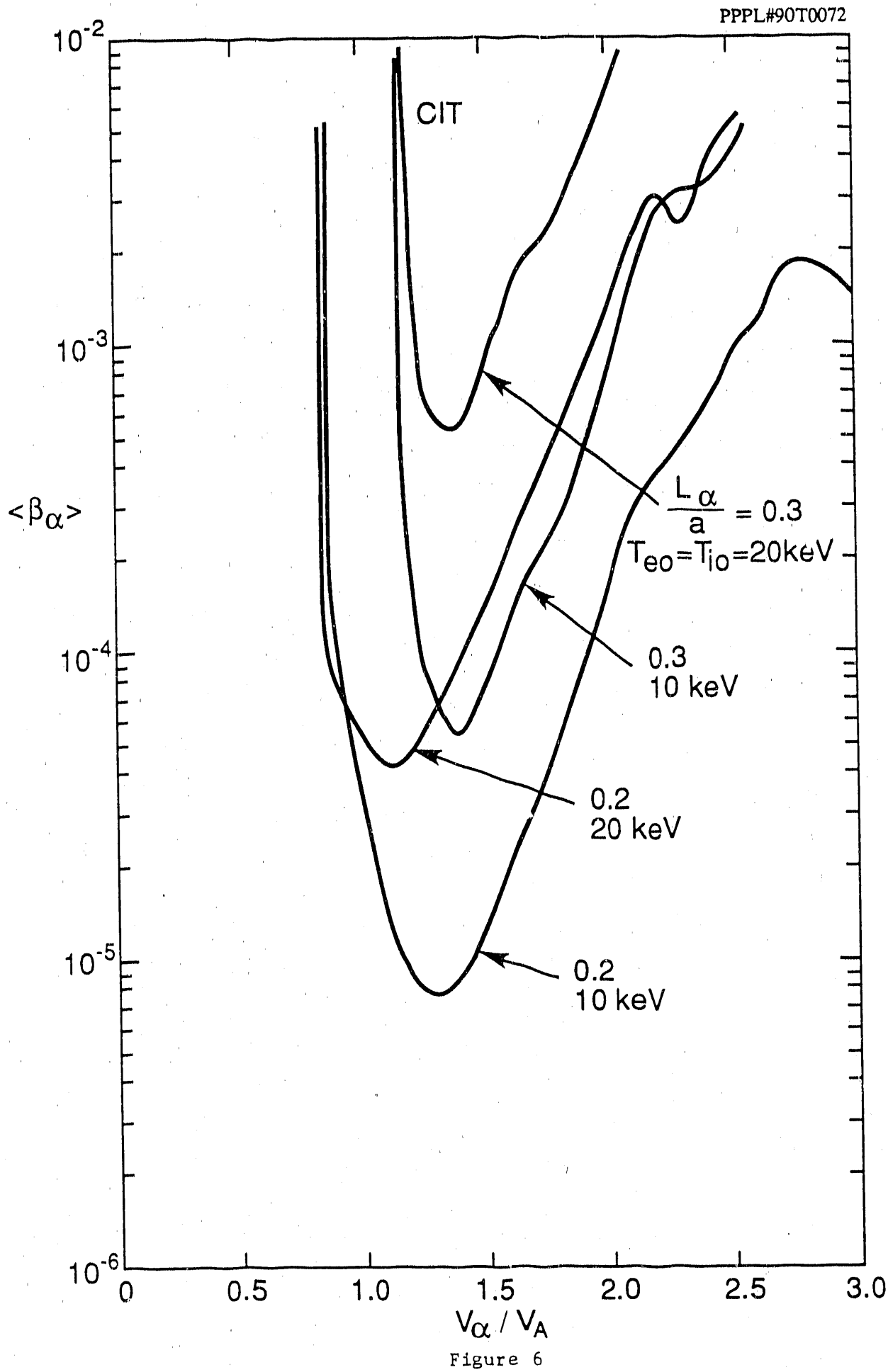
PPPL#90T0072
10^{-2}
10^{-3}
10^{-4}
10^{-5}
10^{-6}
$<\beta_\alpha>$
CIT
$\frac{L_\alpha}{a} = 0.3$
$T_{eo}=T_{io}=20keV$
0.3
10 keV
0.2
20 keV
0.2
10 keV
0
0.5
1.0
1.5
2.0
2.5
3.0
V_α / V_A

Figure 6

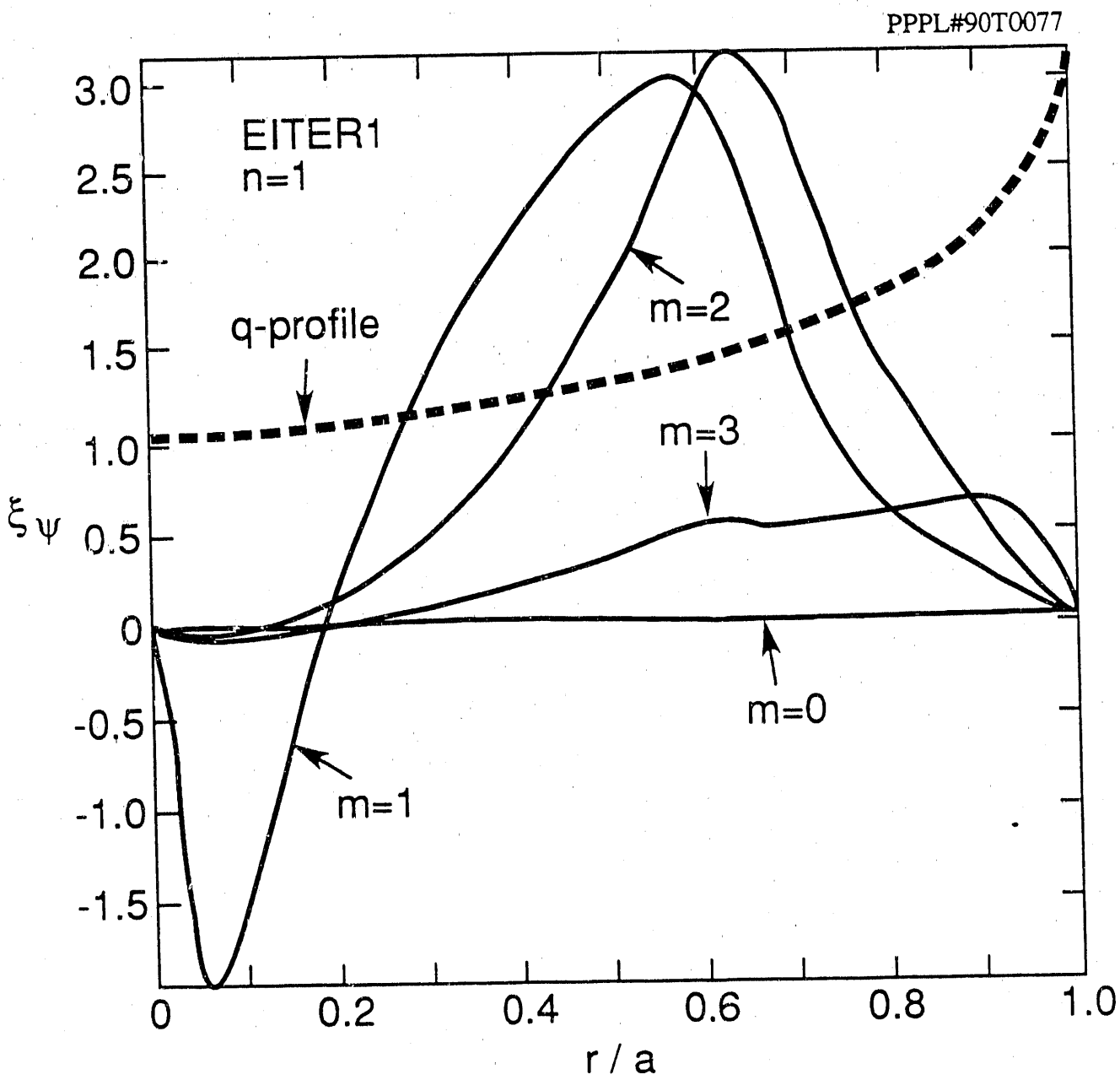
PPPL#90T0077
EITER1
n=1
q-profile
m=2
m=3
m=0
m=1
ξ_ψ
3.0
2.5
2.0
1.5
1.0
0.5
0
-0.5
-1.0
-1.5
0
0.2
0.4
0.6
0.8
1.0
r / a

Figure 7

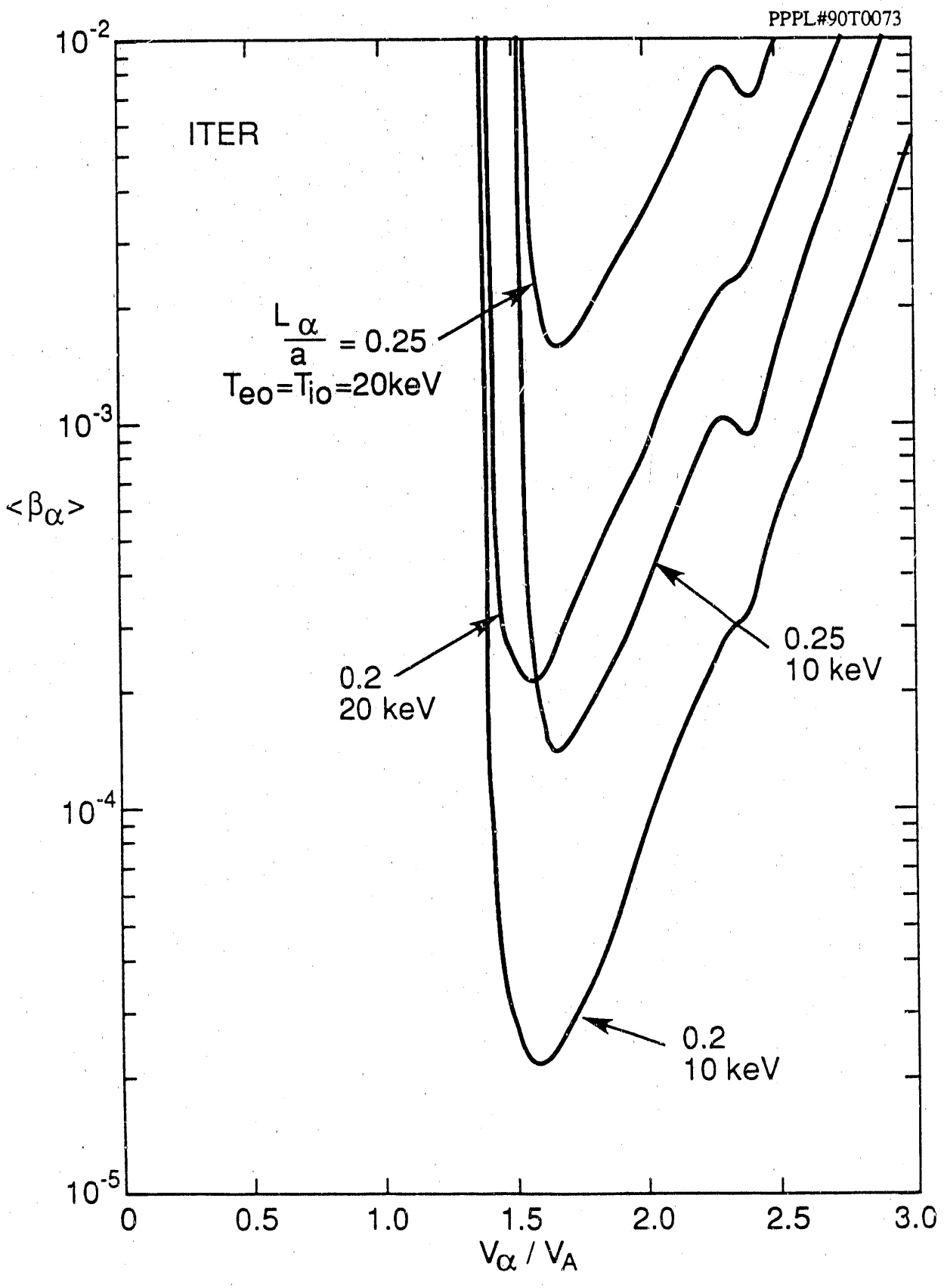
PPPL#90T0073
ITER
$\frac{L_\alpha}{a} = 0.25$
$T_{eo}=T_{io}=20keV$
0.2
20 keV
0.25
10 keV
0.2
10 keV
$<\beta_\alpha>$
10^{-2}
10^{-3}
10^{-4}
10^{-5}
0
0.5
1.0
1.5
2.0
2.5
3.0
V_α / V_A

Figure 8

END

DATE FILMED

11 / 1 / 90